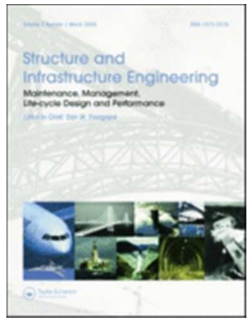

Implications of subsoil-foundation stiffness on the dynamic characteristics of a monitored bridge

Journal:	*Structure and Infrastructure Engineering*
Manuscript ID	NSIE-2017-0368.R2
Manuscript Type:	Original Paper
Date Submitted by the Author:	04-Jun-2018
Complete List of Authors:	Faraonis, Periklis; Aristotle University Thessaloniki, Greece, Department of Civil Engineering Sextos, Anastasios; Aristotle University Thessaloniki, Greece, Department of Civil Engineering; University of Bristol Department of Civil Engineering Papadimitriou, Costas; University of Thessaly, Department of Mechanical Engineering Chatzi, Eleni; Institute of Structural Engineering ETH Zürich, Department of Civil, Environmental and Geomatic Engineering (D-BAUG) Panetsos, Panagiotis; Egnatia Odos S.A
Keywords:	Bridges, Monitoring, Soil dynamics, Identification, Calibration, Finite element method

Note: The following files were submitted by the author for peer review, but cannot be converted to PDF. You must view these files (e.g. movies) online.
NSIE-2017-0368.R2-Figures.rar

Implications of subsoil-foundation modelling on the dynamic characteristics of a monitored bridge

Periklis Faraonis[a], Anastasios Sextos[b*], Costas Papadimitriou[c], Eleni Chatzi[d] and Panagiotis Panetsos[e]

[a]*Department of Civil Engineering, Aristotle University of Thessaloniki, 54124, Thessaloniki, Greece, pfaraonis@civil.auth.gr;*

[b]*Department of Civil Engineering, Aristotle University of Thessaloniki, 54124, Thessaloniki, Greece, asextos@civil.auth.gr & University of Bristol, BS8 1TR, Bristol, United Kingdom, a.sextos@bristol.ac.uk;*

[c]*Department of Mechanical Engineering, University of Thessaly, 38334, Volos, Greece, costasp@mie.uth.gr;*

[d]*Department of Civil, Environmental and Geomatic Engineering, Swiss Federal Institute of Technology in Zurich, Wolfgang Pauli Str.15, Zurich, Switzerland, chatzi@ibk.baug.ethz.ch;*

[e]*Egnatia Odos S.A, 57001, Thermi, Greece, ppane@egnatia.gr*

[*] corresponding author

Abstract

Model updating based on System Identification (SI) results is a well-established procedure to evaluate the reliability of a developed numerical model. In this inverse assessment problem, soil-foundation compliance is often not explicitly considered rigorously during design and/or purely numerical assessment. The present work aims to investigate the correlation between subsoil-foundation stiffness and modal characteristics of bridges, as a means to identify a threshold beyond which rigorous subsoil modelling is a prerequisite for reliable model updating. The 2nd Kavala Ravine bridge, in Greece, serves as the case study for this purpose for which a reasonably reliable finite element (FE) model is developed and updated based on ambient vibration measurements. Alternative soil profiles and subsequently redesigned foundation systems are then used to examine the effect that the correspondingly variable soil compliance would have on the natural frequencies of the bridge. It is shown that soil stiffness alone is not an adequate proxy to decide on the necessity for subsoil modelling, as the foundation stiffness (particularly in cases of softer soil profiles) tends to balance the dynamic properties of the holistic soil-foundation system. The soil-foundation stiffness is therefore the key parameter that dictates the need for refined modelling of soil-structure interaction in the framework of SI-based model updating.

Keywords: Bridges; monitoring; soil dynamics; identification; calibration; finite element method.

Introduction

System Identification serves as an increasingly useful for assessing the structural health of infrastructure systems, which operates supplementary to visual inspection and to other non-destructive evaluation techniques (Chang, Flatau & Liu, 2003). It aims to provide insight into the current health state of a structure and/or its residual lifetime, commonly by detecting alteration in vibration properties (mainly natural frequencies and mode shapes) that are indicative of damage. The latter may be identified either via: (i) output-only ambient vibration-based system identification techniques, where only the structural response is recorded (Peeters & De Roeck ,1999; Brincker, Zhang & Andersen , 2001; Gauberghe, 2004), or (ii) input-output methods, where both the response and the excitation are measured (Werner, Beck & Levine, 1987; Chaudhary, Abé, Fujino & Yoshida, 2000; Seo, Hu & Lee, 2016). One approach is to follow the evolution of the identified modal properties during the structure's operation (Dervilis, Worden & Cross, 2015; Spiridonakos, Chatzi & Sudret, 2016; Reynders & De Roeck, 2009), to investigate whether observed variations can be attributed to structural stiffness degradation. When long-term monitoring data is unavailable, which is the most common case, the identified modal properties can be compared with finite element (FE) model predictions. Appropriate model updating is then applied, until a correlation is achieved between the identified and numerically calculated modal characteristics (Mottershead & Friswell, 1993). This procedure may draw important information regarding both the structural integrity and the reliability of the nominal FE numerical model of the 'as-built' structure.

Several studies have demonstrated that apart from damage-related stiffness degradation, deviations between the identified and the reference modal properties may be also attributed to soil-structure interaction (SSI) effects. Luco (1980), identified shifts of the soil-structure stiffness of the nine-story reinforced concrete Milikan library in California, during the 1971 San Fernando earthquake (notably, period elongation was partially recovered at the end of ground shaking). Todorovska (2009), further studying measurements from the same building between 1970 and 2002, quantified the amplitude-dependence of the system frequency. This was driven by the fact that during the strongest Whittier-Narrows 1987 earthquake, the system frequency decreased by 40%, finally recovering to 15% decrease, compared to the initial state of 1970. In Trifunac, Ivanovic and Todorovska (2001b), the amplitude dependence of system frequency of a seven-story reinforced concrete hotel in Van Nuys, California was studied based on recordings from 12 earthquakes. The observed changes were attributed to both the geometric nonlinear response of the foundation-soil system (in terms of the idealised depth of foundation fixity) and to variation of soil properties due to consolidation induced by low amplitude aftershocks. The authors highlighted the importance of modelling soil-foundation systems with sophisticated models as part of Structural Health Monitoring (SHM).

Similarly, Chaudhary et al. (2001, 2008), examined the effect of SSI on the measured properties of permanently monitored bridges in Japan, highlighting higher impact on weaker soils. In that case, the frequency of the flexible base structure was measured half to the corresponding fixed-base, varying as a function of the column to foundation stiffness ratio. An additional 10% to 30% reduction in the shear modulus was observed during earthquake excitation. Lately, in Gomez, Ulusoy and Feng (2013), the modal characteristics of a bridge in California were identified based on six earthquake records, concluding that larger earthquake intensities may result in reduced natural frequencies, due to softening of the foundation soil. It is noted for completeness, that variability in the environmental conditions such as humidity, traffic loading and wind speed may also lead to additional, indeed small but not negligible (up to 5%) discrepancies in the identified dynamic characteristics of bridges (Cross, Koo, Brownjohn & Worden, 2013; Yuen & Kuok, 2010).

Even though the above research has highlighted the importance of soil compliance in the measured properties of both bridges and buildings, only a few studies that utilize system identification data to calibrate finite element models, do account for soil stiffness (see Crouse, Hushmand & Martin, 1987; Huang, Yang, Ku & Chen, 1999; Chaudhary, 2004; Teughels & De Roeck, 2004; Morassi & Tonon, 2008; Sextos, Faraonis, Zabel, Wutke, Arndt & Panetsos, 2016), while others simply adopt the assumption of fixed support conditions (Wu &Li, 2004; Caetano, Cunha, Gattulli & Lepidi, 2005; Jaishi & Ren, 2005; Macdonald & Daniell, 2005; Zivanovic, Pavic & Reynolds, 2009). Admittedly, it is not straightforward to assess in advance neither the necessity of detailed modelling (Chaudhary, 2015; Chaudhary, 2017) nor the accuracy of the fixed-base assumption. This is mainly due to the fact that the dynamic properties of a soil-structure system are inevitably dependent on the intensity of excitation, which is not known in advance and on the salient subsoil conditions which may considerably vary in space.

Along these lines, the scope of this paper is to study numerically the sensitivity of dynamic properties (natural frequencies, modal participating mass ratios and mode shapes), of a permanently monitored bridge structure, on alternative assumptions made regarding its soil-foundation stiffness. Having updated a FE model and studied the dependency of the soil-structure system dynamic properties on the compliance of the supporting subsoil, it is further aimed to determine the conditions under which boundary conditions need to be tuned in order to match the globally measured quantities. To serve the above purpose, existing modal identification data are employed for a well-studied bridge structure in Greece (Ntotsios et al., 2008) that has been continuously monitored since 2005. The methodology adopted, the results obtained, and the observations made for different soil conditions and, subsequently, different bridge foundation configurations are discussed in the following.

Methodology

In FE model updating applications an evolutionary (search) algorithm is commonly utilized to determine the optimal values of a set of n structural parameters $\theta = \{\theta_1, \theta_2, \ldots, \theta_n\}$, of the initially developed numerical model, minimizing a user-defined objective function $J(\theta)$. The scope of the herein applied FE model updating scheme, is to calibrate the nominal numerical model until its numerically predicted natural frequencies and mode shapes $\{\omega_r(\theta),\ \varphi_r(\theta),\ r=1,\ldots,m\}$ adequately approximate the experimentally obtained modal characteristics $\{\hat{\omega}_r(\theta),\ \hat{\varphi}_r(\theta),\ r=1,\ldots,m\}$, where m is the number of modes of interest. The objective function $J(\theta)$ of Equation (1) is therefore formed to represent an overall measure of fit between the measured and the model predicted modal characteristics:

$$J(\theta)=\sum_{r=1}^{m}\left[\frac{\left[\omega_r(\theta)-\hat{\omega}_r\right]^2}{\left[\hat{\omega}_r\right]^2}\right]+w\sum_{r=1}^{m}\left[1-\left|MAC_r(\theta)\right|\right] \qquad (1)$$

where, the first term represents the measure of fit between the identified and the model-predicted frequency for the r^{th} mode, while the second term represents the difference between the measured and the model-predicted eigenvector for the r^{th} mode, through the modal assurance criterion (MAC):

$$\left|MAC_r(\theta)\right|=\frac{\left|\phi_r(\theta)^T\times\hat{\phi}_r\right|^2}{\left\|\phi_r(\theta)\right\|\times\left\|\hat{\phi}_r\right\|} \qquad (2)$$

Furthermore, the weighting factor $w,\{0\le w\le 1\}$ in Equation (1), defines the level of contribution of the second term in the model updating result. Given that the weighting factor w, controlling the relative importance of the modal shape matching, is inevitably subjective, three alternative case scenarios were investigated as shown in Table 1: (i) $w=1$ for case A, (ii) $w=0.5$ for case B, and (iii) $w=0$ for case C.

The covariance matrix adaptation evolution strategy (CMA-ES) algorithm (Hansen, Müller & Koumoutsakos, 2003) was selected for the minimization of the objective function $J(\theta)$. The heuristic nature of the algorithm allows tackling of non-conventional optimization problems (non-linear non-convex black-box optimisation) and can be applied both to unconstrained and bounded constraint continuous optimization problems. It is a second order approach estimating, within an iterative procedure, a covariance matrix, for convex-quadratic functions closely related to the inverse Hessian. This renders the method applicable to non-separable and/or badly conditioned problems. In contrast to quasi-Newton methods, the CMA-ES neither computes nor uses gradients. Thus, the method is efficiently applied on problems for which the gradients are not available or are inconvenient to compute.

Herein, the CMA-ES was selected to be used since it offers a convenient, though computationally more costly alternative, to solve the opitimization problem. Even though in our case the objective function is smooth and continuous (Figure 1), CMA-ES can be also efficiently applied on non-smooth and even non-continuous problems, as well as on multimodal and/or noisy problems (Hansen & Ostermeier, 2001; Hansen & Kern, 2004). A comparative assessment regarding the efficiency of the selected algorithm with respect to other available options is presented in a following section.

It is noted that as the objective of the postulated parameterization was to calibrate the properties of individual elements such as the modulus of elasticity of the bridge bearings, deck and piers to match the identified modal characteristics of the structure, local changes or spatially variability of soil stiffness was not considered. This would also require a much denser array of sensors and hence, it was deemed as falling outside the scope of this study.

Description of the studied bridge

The 2nd Kavala bypass Ravine bridge is studied herein, located along the Egnatia

Motorway, which is major lifeline crossing the northern Greece from its western to its eastern border (Figure 2). The construction of the bridge was completed in 2004 and its total length is approximately 180m. The structural system comprises of two statically independent branches, with four identical simply supported spans of 45m (Ntotsios et al., 2008). Each span is built with four precast post-tensioned I-beams of 2.80m height that support a continuous deck of 26cm thickness and 13m width. The four spans of the deck are interconnected through a 2m long and 20cm thick continuity slab over the piers (details in Figure 2). The I-beams are supported by two abutments (A_1 and A_2) and by three piers (M_1, M_2 and M_3) through laminated elastomeric bearings. Each abutment has 4 circular bearings (Φ650×195mm) and each pier has 8 rectangular bearings (600×400×99mm for M_1 and M_3, 600×300×52mm for M_2).

The piers have a 4×4m hollow cross-section with 40cm wall thickness and heights equal to 26.50m (M_1, M_3) and 48.90m (M_2). All piers are supported on 6m diameter solid concrete caissons, of 10m, 9.80m and 12.20m length (M_1, M_2, M_3, respectively), embedded into the subsoil. Based on the geotechnical report of the bridge and 5 boreholes at the two abutments and the base of piers M1-M3, the soil was described as volcanic rocks, in particular felsic granite and shale with a Rock Mass Rating RMR of 40 (poor), and a Rock Quality Designation index RQD<25% (very poor). Given a uniaxial compressive strength σ_c=40MPa, the Young's modulus of elasticity E_0 is identified equal to 3.5GPa based on the following expression (Hoek & Brown, 1997):

$$E = \sqrt{\frac{\sigma_c}{100}} 10^{\left(\frac{RMR-10}{40}\right)} \tag{3}$$

The shear wave velocity V_{S0} was computed to be 820m/sec (for Poisson ratio v =0.3 and mass density ρ=2 t/m^3) also corresponding to rock, according to the Eurocode 8 soil classification (rock, type A $V_{S,30}$> 800m/sec):

$$V_{S0} = \sqrt{\frac{G_0}{\rho}} = \sqrt{\frac{E_0 2(1+v)}{\rho}} \tag{4}$$

Notably, even though the subsoil of the studied bridge was very stiff, the bridge was not founded on shallow foundation but using large caissons. This was due to the fact that the foundation slope was very steep with a high landslide susceptibility, hence, constructability and accessibility eventually dictated the design.

Identified structural modes via ambient vibrations

The structural modes of the southern branch of the 2nd Kavala bypass Ravine bridge were already identified via low amplitude (8mg maximum measured acceleration in the horizontal direction and 43mg in the vertical direction) ambient vibrations by Ntotsios et al. (2008). More specifically, the bridge was instrumented with 24 uniaxial Kinematrics Episensor accelerometers (±2 g full scale), as shown in Figure 3. The first letter in the sensor labels denotes their orientation (L: longitudinal, T: transverse, V: vertical), while the last their number. From the total of 24 accelerometers, 18 were installed on the deck (2 longitudinal, 10 vertical and 6 transverse), and 6 at the top of the three piers.

The methodology adopted to identify the structural modes via ambient vibrations was based on a least squares minimization of the measure of fit between the cross power spectral density (CPSD) matrix $\hat{S}(k\Delta\omega;\psi) \in C^{N_0 \times N_0}$ and the CPSD matrix, $S(k\Delta\omega;\psi) \in C^{N_0 \times N_0}$ where N_0 is the number of measured degrees of freedom (DOF), $\Delta\omega$ is the discretization step in the frequency domain, $k = \{1,...,N_\omega\}$ is the index set corresponding to frequency values $\omega = k\Delta\omega$, N_ω is the number of data in the indexed set, and ψ is the parameter set to be estimated. In Equation (5) the $\hat{S}(k\Delta\omega;\psi)$ matrix was estimated from the measured output acceleration time histories, while the

$S(k\Delta\omega;\psi)$ matrix was predicted by a modal model using general (non-proportional) viscous damping (Cauberge, 2004; Brincker & Ventura, 2015):

$$E(\psi)=\sum_{k=1}^{N_\omega} tr\left[S(k\Delta\omega;\psi)-\hat{S}(k\Delta\omega)^{*T}\left(S(k\Delta\omega;\psi)-\hat{S}(k\Delta\omega)\right)\right] \quad (5)$$

Eventually, in the work of Ntotsios et al. (2008) seven mode shapes (Figure 4a) were reliably identified; three transverse modes, one longitudinal and three bending modes of the deck. Their respective natural frequencies were in the range of 0.81Hz-3.51Hz, as shown in Table 1 and they were deemed representative of the structural dynamic response since additional measurements conducted under alternative environmental conditions in terms of temperature and humidity led to similar modal data with a discrepancy of less than 2%.

Numerical modelling

Geometry and assumptions

A detailed FE model of the Kavala bridge was developed in ABAQUS 6.14 (Figure 4b), to numerically predict the modal characteristics of the bridge. In contrast to the, two-node, beam-type finite elements used in the initial work of Ntotsios et al. (2008), this model used three-dimensional, eight-node, brick-type finite elements (C3D8 type in ABAQUS) to simulate the subsoil and all the structural components of the bridge including the deck, I-beams, piers, bearings, caissons and abutments. The prestress forces in the girders were not simulated on the grounds of not significantly affecting the dynamic behaviour of prestressed beams (Hamed & Frostig, 2006). Overall, the numerical model consists of approximately 247,000 hexahedral brick elements that correspond to 407,000 degrees of freedom. The mesh size was set equal to 0.75m for the elements modelling the concrete sections, 0.25m for the bearings and 2m for the large volume of soil.

Prior to the development of the FE model, an in-situ measurement of the bridge geometry was performed to verify the drawings and update the 'as-built' condition of the structure. All materials are numerically assumed to be elastic, isotropic and homogenous. Their nominal, uncracked values are given in Table 2. The subsoil static stiffness E_0, was considered equal to 3.5GPa, based on the geotechnical investigation report. The elastomeric laminated bearings are horizontally anchored at both ends through friction under both operational and vibration monitoring conditions. However, due to the high friction coefficient between the bearing and the top and bottom reinforced concrete surfaces, the assumption of a full bong was made and the Abaqus "tie" constrain type was used.

For the abutment backfill, a well compacted material was adopted with a Young's modulus equal to 60MPa (Taskari & Sextos, 2015). The volume of the soil surrounding the caissons that was modelled was $2H_C \times 6D_C \times 6D_C$, where H_C and D_C denote the caisson height and diameter respectively (Figure 5). The abutment foundation soil volume modelled was $5W_A \times 62L_A \times l$, with W_A being the abutment width, L_A the abutment height and l the abutment plus the embankment length l_E (Figure 6). The latter was taken equal to 30m, that is, well beyond the L_c=17.8m critical embankment length which was estimated analytically for an embankment slope $1/S = 1/3$, embankment breadth B_c=27m and embankment height H=8m according to Zhang and Makris (2002):

$$L_c \approx 0.7\sqrt{SB_cH} \qquad (6)$$

All foundation soil volumes were externally restricted in the transverse and longitudinal direction (x and y) to account for the adjacent subsoil, leaving the vertical displacement along the z unrestrained, while being fixed at their base. Absorbing boundary conditions were not considered in the analysis since it was only modal analysis that was employed without response in the time domain. A sensitivity analysis was carried out to verify that the geometry of the selected soil mass did not affect by more than 2% the predicted dynamic characteristics in comparison to an extensively refined FE model where the entire valley was modelled (Figure 7).

Modal analysis

The numerically predicted dynamic characteristics of the three-dimensional FE model described above were compared with the structural modes identified via ambient vibrations by Ntotsios et al. (2008). As it is evident by the results summarized in Table 1 (Column 2), the initially developed numerical model fails to predict the measured response, as it exhibits large deviations from the identified modal frequencies. More specifically, the initial FE frequency prediction is approximately 55% lower than the measured one in the longitudinal direction, and about 33% - 58% lower in the transverse direction. In general, it is observed that the modes predicted by the initial 3D FE model are on average 32% lower than those measured via ambient vibrations, thus, the real structure is identified as being significantly stiffer. This is mainly attributed to the fact that the stiffness values used for the initial FE prediction were based on the bridge design brief, which correspond to high levels of shear strain that are expected to occur in case of the design earthquake (Yura, Kumar, Yakut, Topkaya, Becker & Collingwood, 2001).

Model updating framework

Given the above discrepancies between the identified (i.e., measured) and the numerically predicted natural frequencies and the predicted response, a finite element model updating framework was deemed necessary to reduce the observed error. The parameters that were considered to be uncertain and assumed to potentially affect the efficiency of the initial 3D FE model (Table 3) were: (i) the Young's modulus of elasticity of the superstructure, including the deck and the I-beams, hereafter termed θ_{deck} , (ii) the modulus of elasticity of the piers, θ_{piers} , (iii) the modulus of elasticity of the bearings used for the abutment and piers, θ_{bear} and (iv) the stiffness of the backfill θ_{back} . Note that the since the bearings are fully modelled using 3D (solid) elements, it is the Young's modulus of the rubber that is to be updated (considering the modulus of the steel plates constant) and not the shear modulus of the entire bearing that is typically used in case the bearing is modelled with a 1D shear spring. Further, θ is defined as the aspect ratio of the updated over the initial parameter values, thus, the initial (nominal) FE model corresponds to parameter values $\theta = 1$. It is clarified that the influence of the backfill stiffness θ_{back} was found negligible as shown in Figure 1. This is due to the presence of the 25cm expansion joint between the deck and the abutment, and the fact that the force transfer to the abutment is made through the bearing only, being almost directly transferred to the rock in which the abutment is founded.

The same applies to the subsoil Young's modulus, which was not updated, since its high value (3.5GPa) almost corresponds to fixed-base conditions. Sensitivity analyses confirmed that even a ±50% variation around its mean value did not affect the modal characteristics of the bridge. In fact, this was the primary reason for studying the particular bridge, since its stiff soil conditions reduce the epistemic uncertainty associated with model updating of the superstructure so that the soil stiffness itself can then be only varied parametrically numerically for comparative investigation of different soils and foundations. As shown in Table 3, the significant parameters to be updated are assumed to be bounded within prescribed ranges of variation (i.e., $0.70<\theta_{deck}<1.30$, $0.70<\theta_{piers}<1.30$ and $1<\theta_{bear}<15$), to avoid updating solutions that lack physical meaning. The justification for these bounding values is presented below.

Pier and deck constraints

There is a series of factors that may affect the modulus of elasticity of concrete that is identified using ambient vibrations in relation to its actual design value. First, the nominal design value of concrete is not calculated based on the results of compression tests of cored concrete samples but is instead assumed equal to the mean elastic modulus of concrete (E_{cm}). Compression tests of cored concrete samples usually display a ±10% covariance of the concrete Young's modulus compared to the E_{cm}. Moreover, according to the definition of the E_{cm} in Eurocode 2, this is calculated for higher strain levels (i.e., strain levels that correspond to 40% of concrete's mean compressive strength) than those developed under ambient vibrations. Additionally, concrete strength increases with time due to aging and this further increases its stiffness, for instance, by 5%-10% in 4 years, for the case of E_{cm}=34GPa, as defined in Eurocode 2. Overall, the identified modulus of elasticity of concrete can be indeed identified higher than the nominal one, however, this increase shall not exceed 30% in total, hence, an upper bound for Young's modulus equal to 1.3 is deemed reasonable.

On the other hand, limited cracking in concrete sections induced by traffic loads, can also decrease their stiffness after some years of bridge operation. More extensive cracking could be further identified for structures that experienced earthquake excitations depending on their intensity. Considering that the bridge studied did not experience any strong earthquake event since its construction in 2004, one shall not expect any decrease to the concrete Young's modulus by more than 10%. In any case, the lower bound for concrete Young's modulus was set to 0.7 to account for any other, potentially unknown, source of damage.

Bearing constraints

Based on similar studies of base-isolated bridges (Chaudhary et al., 2001; Ntotsios et al., 2008) and buildings (Stewart , Conte & Aiken, 1999), it is evident that at low level of excitation, such as ambient vibrations, the identified values of the bearing stiffness can be up to 2-10 times greater than their nominal design ones. This is mainly due to the constitutively different nonlinear behaviour of bearings at small (serviceability) shear strain levels (γ<100%) and the ones expected during an earthquake ground motion (100%<γ<200%) that essentially dictate their design. Another reason for identifying higher bearing stiffness compared to their nominal one is additional friction mechanisms, dislocations, aging, corrosion, humidity, etc. Based on the above considerations, bearing stiffness was bounded between 1 to 15. Notably, a lower bound below unity was not considered since the bridge was rather new and bearing damage was not deemed probable at least to such an extent that it would override the difference between ambient and earthquake vibration.

Effect of alternative weighting factors on model updating results

The natural frequencies of the updated numerical models of the Kavala bridge are presented in Table 1. Three cases are examined with different weighting factors for mode shape and natural frequencies matching (i.e., for case A the weighting factor w, is considered equal to 1, for case B equal to 0.5 and for case C equal to 0). It can be observed that all the investigated model updating cases provide natural frequency estimates that are in good agreement with those identified via ambient vibration measurements. The average error in the natural frequencies is now reduced from 32.34%

to 1.89% for case A, to 1.78% for case B and to 1.72% for case C. Regarding the identified and the numerically predicted mode shapes, good agreement is also observed, since the MAC values at all three cases are close to 1, for all 7 considered modes.

The optimal values of the significant structural parameters that were updated in order to reduce the initially observed discrepancies in the dynamic characteristics of the initial (nominal) FEM, are summarized in Table 3. It can be observed that the three cases conclude to consistent results, regarding the Young's modulus of elasticity E of the superstructure (θ_{deck}=1.19-1.21) and the bearings' E modulus (θ_{bear}=11.63-11.99). On the contrary, greater, though not excessive, deviation was predicted for the E modulus of the piers, (θ_{piers}=1.12-1.25), showing that the θ_{piers} optimal value depends on the assumption made for the w weighting factor and the contributionof the mode shapes in the objective function $J(\theta)$.

Taking into consideration that the three, equally legitimate, model updating cases provide equally reliable results, but lead to different estimation of the piers' stiffness, an investigation was made, to examine the reliability of the three estimations (12%, 18% or 25% concrete stiffness increase). There are two things that need to be checked. One is whether the non-damage prediction is valid in a seismic prone area, as that of the bridge studied, and secondly to interpret the source of the identified stiffness increase. Along these lines, data were collected from the national observatory of Athens database regarding the strong motion events (M_S>4) that had taken place at the vicinity of the bridge for the period between 2004 (bridge construction year) and 2008 (when ambient vibration measurements took place). It was found that the strongest earthquake occurred in 2007, at an epicentral distance R of 40km, with an M_S=4.5 magnitude. The attenuation laws of Skarlatoudis et al., (2003), eq. (7), and of Theodulidis and Papazachos (1992), eq. (8), proposed for Greece, were then utilized in order to predict the peak horizontal ground acceleration (PGA) that was developed near Kavala bridge during the earthquake of 2007:

$$\log(PGA) = 1.07 + 0.45M_S - 1.35\log(R+6) + 0.09F + 0.06S \pm 0.286 \qquad (7)$$

$$\ln(PGA) = 3.88 + 1.12M_S - 1.65\log(R+15) + 0.41S + 0.71P \qquad (8)$$

where, F is the fault mechanism parameter with value 0 for typical fault mechanisms, S is the site class parameter with value 0 for the Kavala bridge subsoil (rock, type A, $V_{S,30}$ > 800m/sec, based on the Eurocode 8 ground classification) and P is 0 for 50 percentile value and 1 for 84 percentile value. Consequently, the PGA induced by the 4.5 M_S earthquake of 2007 on Kavala bridge, is expected to have been in the range of 0.004g-0.03g, which is deemed inadequate to have produced any substantial stiffness degradation to the Kavala piers.

A series of in-situ non-destructive Schmidt rebound hammer tests were then performed (data from 2016), to validate the model updating results that suggest 12%-25% increase to the piers' Young's modulus of elasticity. More specifically, 160 rebound hammer measurements were conducted at the base of M_1 and M_3 piers (4 set of tests per pier side × 10 measurements per set × 4 pier sides), finally leading to an average rebound value R of 39.1 and 38.1 for M_1 and M_3 piers, respectively. Based on the rebound hammer graph, those R values correspond to characteristic compressive strength f_{ck} equal to 41.60MPa for M_1 and 40MPa for M_3. Eventually, the M_1 and M_3 piers' Young's modulus of elasticity were predicted equal to 35.56GPa and 35.22GPa, respectively, according to Eurocode 2:

$$E_{cm} = 22\left(\frac{f_{ck}+8}{10}\right)^{0.3} \qquad (9)$$

The results of the Schmidt rebound hammer indicate a 17% increase at the piers' nominal E=30GPa modulus and are in closer agreement with the 18% increase, predicted by case B of model updating.

Based on the above detailed justification and considering that the two measurements (ambient vs. Schmidt tests) were conducted under similar temperature conditions (10ºC), the second model updating scenario (case B with a 'balanced; weighting factor w=0.5) is deemed more reliable and is used thereafter.

Effect of alternative optimization algorithms

An investigation is next presented to compare the results obtained from the covariance matrix adaptation evolution strategy (CMA-ES) algorithm with those obtained using different algorithms available within the Matlab environment. For this, the model updating framework, described in the previous sections, was repeated with three alternative Matlab local optimization algorithms: (i) *fmincon interior- point* and (ii) *fminunc quasi-Newton,* that are gradient based algorithms, as well as (iii) *fminsearch* that is a gradient-free method that uses the simplex search method (Lagarias, Reeds, Wright & Wright, 1998). The optimal results obtained by the CMA-ES algorithm (Table 3, case B) are then comparatively assessed with the optimal solutions obtained by the three alternative algorithms (*fmincon*, *fminunc* and *fminsearch*).

As illustrated in Figure 10 and Table 4, *fmincon* and *fminunc* converges prematurely in a neighbourhood of the optimum obtained by CMA-ES, failing to give accurate estimates of the model parameters (see Table 4), mainly due to the fact that the gradients are estimated numerically. Analytical estimation of the gradients to improve the estimates of gradient-based optimization algorithms is possible for special cases of model parameterization but it was not pursued further in this manuscript. On the other hand, *fminsearch* converges to the same solution as CMA-ES with a significantly lower computational effort (187 evaluations compared to 300). Even though this investigation has highlighted the computational advantages of *fminsearch*, employment of CMA-ES was finally deemed necessary to ensure that the global optimum could be obtained and to verify that the *fminsearch* solution was not a local minimum.

Effect of alternative soil-foundation conditions

Soil-foundation stiffness assumptions

Having established a level of confidence regarding the dynamic behaviour of the 2nd Kavala bypass bridge and selecting the most suitable weighting factor and optimization algorithm for the purposes of this study, a parametric analysis was then performed, utilizing the more reliable (as shown in the previous Section) updated numerical model FEM B (Table 1 and Figure 4b). In this parametric analysis, the actual subsoil stiffness (V_{S0}=820 m/sec or E_0=3.5 GPa) was gradually numerically reduced in order to investigate how the dynamic characteristics in terms of natural frequencies, mode shapes and modal participation mass ratios of the Kavala bridge studied would be influenced. Three alternative types of soil profiles were investigated, according to the Eurocode 8 ground classification, namely: rock (type A, $V_{S,30}$> 800m/sec), dense sand, gravel or stiff clay (type B, 360m/sec < V_{S0}< 800m/sec) and deep deposits of dense to medium sand (type C, 180m/sec < $V_{S,30}$< 360m/sec). The soil stiffness of the aforementioned profiles corresponds to small (γ <10^{-6}) soil strain levels induced under ambient vibrations. Extremely soft soil conditions (type D, $V_{S,30}$< 180m/sec) require different foundation systems and/or soil improvement and were not considered in the parametric study.

For the three alternative soil profiles studied herein (namely, types A, B and C) three different foundation systems had to be designed. For the reference case of the rock soil profile (type A), the actual foundation system of the bridge was kept unchanged, whereas for the other two soil profiles (B and C) the foundation system was redesigned according to the Eurocodes 7 and 8 (Figures 8 and 9), assuming that there were no constructability limitations of the actual case study, such as the steep slope and landslide susceptibility. The design quantities are indicatively summarized in Table 5 and Table 6, derived through response spectrum analysis of the soil-bridge system for each soil type as per Eurocode 8, adopting a behaviour factor q=1.8 based on the actual superstructure design and a peak ground acceleration of 0.16g, which is the design seismic acceleration at the site of interest.

The three resulting foundation configurations are summarized below:

- Soil type A (actual, reference case): 6m diameter caissons of 9.80-12.20m length (Figure 5).
- Soil type B (20m of dense sand down to the bedrock level): 7x7x2 rectangular shallow foundation (Figure 8).
- Soil type C (20m of medium-dense sand over 5m of soil B and a bedrock at a depth of -25m): 3x3 pile group of 1m diameter at a spacing over diameter ratio S/D=2.0 with 23m length connected to a 6x6x2 pile cap, embedded by 3m into the stiffer subsoil B (Figure 9). Soil type B was assumed for the foundation subsoil of the abutments.

The water table was ignored in all cases.

Modal characteristics for alternative soil profiles

Having updated the FE model for soil A (FEM B) and redesigned the foundation for soils

B and C, the anticipated natural frequencies f of the Kavala bridge, calculated numerically for the three studied soil profiles, were normalized to the natural frequencies $f*$, calculated with the updated numerical model FEM B (Table 1) that considers the actual rock soil conditions (V_{S0}=820 m/sec, type A) of the bridge. Therefore, the ratio $f/f*$, in Figure 11, can be interpreted as a soil-structure interaction index, illustrating how the reduction of soil stiffness in terms of shear wave velocities affects the natural frequencies of Kavala bridge. It is observed that, as anticipated, the natural frequencies of the seven considered mode shapes reduce as soil stiffness reduces. Specifically, the natural frequencies of the Kavala bridge reduce up to 8% for type B (360m/sec < $V_{S,30}$< 800m/sec) of soil conditions founded on shallow foundations and up to 12% for type C (180m/sec < $V_{S,30}$< 360m/sec) of soil conditions founded on a pile group.

The influence of soil compliance on the modal participating mass ratios of Kavala bridge as computed using the modal analysis results of the developed FE models, is further shown in Figure 12. This figure illustrates that for type A rock soil and caisson foundation, 78% of the structural mass is activated by the first transverse mode (T1), 91% by the first longitudinal mode (L1) and 33% by the first bending mode (B1) of the deck. It is also shown that the reduction of soil stiffness for the case of soil type B with a shallow foundation or type C with a pile group, is not expected to influence significantly (<1%) the modal participation mass ratios in the transverse degree of freedom (u_y) associated with mode T1 and longitudinal degree of freedom (u_x), associated with mode L1. On the contrary, an approximately 30% increase is predicted for the modal participating mass ratios in the vertical degree of freedom (relevant to mode B1), for the softer, type C, soil profile.

The Kavala bridge modal vectors, predicted for the actual soil conditions ($V_{S,30}$ =800 m/sec, type A, rock), are compared in Figure 13 with those predicted for the alternative values of $V_{S,30}$ (for soils B and C), to examine the influence of soil compliance on the mode shapes of Kavala bridge. The MAC criterion is used to calculate the mode shapes correlation of the alternative soil compliant scenarios. For low ambient vibrations, where soil strain is less than 10^{-6}, the Kavala bridge mode shapes were not found to vary and deviations were less than 5% for the studied soil profiles (180m/sec < $V_{S,30}$ < 800m/sec).

Summarizing, it can be concluded that Kavala bridge dynamic characteristics as identified by ambient vibrations were not significantly influenced by assuming different soil profiles and subsequently redesigned foundations, except for soil type C (180m/sec < $V_{S,30}$ < 360m/sec) and a pile group foundation, where a variation of 12% was observed. Notably, in case of seismic excitation the potential influence of soil compliance is expected to be significantly higher (Chaudhary et al., 2001), however, this is something that cannot be captured by modal analysis and model updating based on ambient vibration measurements.

Conclusions

The present work examines the potential influence of soil compliance on the numerical predictions of the dynamic characteristics of a bridge in terms of natural frequencies, modal participating mass ratios and mode shapes, in the framework of FE modelling for system identification purposes. It also investigates the conditions under which detailed soil modelling is necessary to achieve a reliable system identification of the studied bridge. To facilitate the above purpose, the 2nd Kavala bypass bridge in Greece is used as a case study. This is a bridge founded on very stiff soil formations through a large caisson foundation, thus minimizing the epistemic uncertainty associated with subsoil modelling. Initially, a reliable FE model of the structure is developed after refined model updating, utilizing ambient vibration measurements. Alternative weighting factors for natural frequencies and mode shape matching are explored along with different optimization algorithms to identify the most suitable approach for the problem studied. Having established a level of confidence for the FE modelling of the piers and superstructure, a parametric numerical analysis is then performed for three alternative soil profiles (type A, B and C according to Eurocode 8 or B, C and D to ASCE 7-10 site classification) and three alternative foundation configurations that are redesigned to Eurocode 7 and 8 involving caissons, shallow foundations and pile groups.

It is shown that for small soil strain levels ($\gamma < 10^{-6}$) that are induced under ambient vibrations, the actual Kavala bridge dynamic characteristics (computed for soil type A, $V_{S,30}$=800 m/sec) do not significantly (<1%) vary when the caissons compliance is accounted for, given that the system, as anticipated, is effectively responding as practically fixed at its base. For the bridge resting on soil type B and shallow foundations, refined FE modelling of the soil-foundation system leads to a variation of less than 10% in the identified natural frequencies. Greater deviations are shown for the case of type C and a pile group foundation, of the order of 12% in terms of natural frequencies, 30% maximum increase in the modal participating mass ratios in the vertical direction and 5% in the mode shape vectors of the three bending modes.

It is therefore shown that during model updating based on the identified natural frequencies and modes of the bridge, the decision to consider subsoil compliance or assume foundation fixity, shall be based on the stiffness of the soil-foundation sub-system of the bridge and not on the properties (i.e., subsoil type) of the soil volume alone, as previously observed by Chaudhary, Abé & Fujino, 2001 . Overall, a ratio of K/K* =

0.90 (i.e., stiffness of the SSI over that of the fixed-base system) can be used as a threshold value beyond which a non-negligible error in the identified modal properties may occur. This ratio is not as low as one would expect considering soil variation only, however, it is restrained by the design practice itself that tends to balance a softer soil formation with a stiffer foundation. Further research is required before making more general statements involving different structural systems and spatially variable or softer soil conditions.

Acknowledgments

The authors would like to thank EGNATIA S.A. highway for providing the design drawings of the bridge studied and to the anonymous Reviewers for their constructive feedback.

References

ABAQUS 6.14 [Computer software]. Pawtucket, RI, Simulia.

ASCE (2010). Minimum design loads for buildings and other structures. ASCE/SEI 7-10, American Society of Civil Engineers, Reston, VA.

Brincker, R., Zhang, L., & Andersen, P. (2001). Modal identification of output-only systems using frequency domain decomposition. *Smart Materials and Structures*, *10(3)*, 441–445.

Brincker, R., & Ventura, C.E. (2015). *Introduction to operational modal analysis*. Germany:Wiley Blackwell.

Caetano, E., Cunha, A., Gattulli, V., & Lepidi, M. (2008). Cable-deck dynamic interactions at the International Guadiana bridge: On-site measurements and finite element modelling. *Structural Control and Health Monitoring*, *15(3)*, 237-264.

Cauberghe, B. (2004). Applied frequency-domain system identification in the field of experimental and operational modal analysis. PhD Thesis, Vrije Universiteit Brussel, Belgium.

Crouse, C.B., Hushmand, B., & Martin, G.R. (1987). Dynamic soil structure interaction of single-span bridge. *Earthquake Engineering and Structural Dynamics*, *15(6)*, 711–729.

Chang, P. C., Flatau, A., & Liu, S. C. (2003). Review paper: Health monitoring of civil infrastructure. *Structural Health Monitoring*, *2(3)*, 257-267.

Chaudhary, M.T.A., Abé, M., Fujino, Y., & Yoshida, J. (2000). System identification of two base-isolated buildings using seismic records. *Journal of Structural Engineering*, *126(10)*, 1187–1195.

Chaudhary, M.T.A., Abé, M., & Fujino, Y. (2001). Identification of soil-structure interaction effects in base isolated bridges from earthquake records. *Soil Dynamics and Earthquake Engineering*, *21(8)*, 713–725.

Chaudhary, M.T.A. (2004). Influence of pier stiffness degradation on SSI in base-isolated bridges. *Journal of Bridge Engineering*, *9(3)*, 287-296.

Chaudhary, M.T.A., & Fujino, Y. (2008). System identification of bridges using recorded seismic data and its application in structural health monitoring. *Structural Control and Health Monitoring*, *15(7)*, 1021-1035.

Chaudhary, M.T.A. (2015). Effect of SSI on modal properties of bridges founded in various soil and rock profiles. *Proceedings of 10th Pacific Conference on Earthquake Engineering*, Sydney, Australia.

Chaudhary, M.T.A. (2017). Seismic response of bridges supported on shallow rock foundations considering SSI and pier column inelasticity. *KSCE Journal of Civil Engineering*, *21(1),* 285-295.

Cross, E.J., Koo, K.Y., Brownjohn, J.M.W., & Worden, K. (2013). Long-term monitoring and data analysis of the Tamar bridge. *Mechanical Systems and Signal Processing*, *35(1-2)*, 16 -34.

Dervilis, N., Worden, K., & Cross, J. (2015). On robust regression analysis as a means of exploring environmental and operational conditions for SHM data. *Journal of Sound and Vibration*, *347*, 279-296.

Egnatia Odos S.A. (2010). *Monitoring and maintenance of 2nd Kavala bypass ravine bridge* (Rep. No. BR04.31.32.2010). Thessaloniki: Egnatia Odos, Greece.

European Committee for Standardization. (2004). Eurocode 2: Design of concrete structures - Part 1-1: General rules and rules for buildings (EN 1992-1-1), Brussels, Belgium.

European Committee for Standardization. (2004). Eurocode 7: Geotechnical design - Part 1: General rules (EN 1997-1), Brussels, Belgium.

European Committee for Standardization. (2004). Eurocode 8: Design of structures for earthquake resistance - Part 1: General rules seismic actions and rules for buildings (EN 1998-1), Brussels, Belgium.

Gomez, H.C., Ulusoy, H.S., & Feng, M.Q. (2013). Variation of modal parameters of a highway bridge extracted from six earthquake records. E*arthquake Engineering and Structural Dynamics*, *42(4)*, 565-579.

Hamed, E., & Frostig, Y. (2006). Natural frequencies of bonded and unbonded prestressed beams -prestress force effects. *Journal of Sound and Vibration, 295(1-2)*, 28-39.

Hansen, N., & Ostermeier, A. (2001). Completely derandomized self-adaptation in evolution strategies. *Evolutionary Computation*, *9(2)*, 159-195.

Hansen, N., Müller, S.D., & Koumoutsakos, P. (2003). Reducing the time complexity of the derandomized evolution strategy with covariance matrix adaptation (CMA-ES). *Evolutionary Computation*, *11(1)*, 1-18.

Hansen, N., & Kern, S. (2004). Evaluating the CMA evolution strategy on multimodal test functions. Proceedings of 8th International Conference on Parallel Problem Solving from Nature, Springer, Heidelberg, Germany.

Hoek, E., & Brown, E.T. (1997). Practical estimates of rock mass strength. *International Journal of Rock Mechanics and Mining Science*, 34(8), 1165-1186.

Huang, C.S., Yang, Y.B., Ku, L.Y., & Chen, C.H. (1999). Dynamic testing and system identification of a multi-span highway bridge. E*arthquake Engineering and Structural Dynamics*, *28(7-8)*, 857-878.

Jaishi, B., & Ren, W. (2005). Structural finite element model updating using ambient vibration test results. *Journal of Structural Engineering*, *131(4)*, 617-628.

Lagarias, J.C., Reeds, J.A., Wright, M.H., & Wright, P.E. (1998). Convergence properties of the Nelder-Mead Simplex method in low dimensions. SIAM Journal of Optimization, 9(1), 112–147.

Luco, E. (1980). Soil-structure interaction and identification of structural models. Proceedings of 2nd ASCE Specialty Conference on Civil Engineering and Nuclear Power, Knoxville, Tennessee, USA.

Macdonald, J.H.G., & Daniell, W.E. (2005). Variation of modal parameters of a cable-stayed bridge identified from ambient vibration measurements and FE modelling. *Engineering Structures*, *27(13)*, 1916-1930.

Mottershead, J.E., &. Friswell, M.I. (1993). Model updating in structural dynamics: a survey. *Journal of Sound and Vibration*, *167(2)*, 347-375.

MATLAB [Computer software]. MathWorks, Natick, MA.

Morrasi, A., & Tonon, S. (2008). Dynamic testing for structural identification of a bridge. *Journal of Bridge Engineering*, *13(6)*, 573-575.

Ntotsios, E., Caracostas, C., Lekidis, V., Panetsos, P., Nikolaou, I., Papadimitriou, C., & Salonikos, T. (2008). Structural identification of Egnatia Odos bridges based on ambient and earthquake-induced vibrations. *Bulletin of Earthquake Engineering*, *7(2)*, 485-501.

Peeters, B., & De Roeck, G. (1999). Reference-based stochastic subspace identification for output-only modal analysis. *Mechanical Systems and Signal Processing*, *13(6)*, 855–878.

Reynders, E., & De Roeck, G. (2009). Encyclopedia of structural health monitoring, Continuous vibration monitoring and progressive damage testing on the Z24 bridge, Wiley, New York.

Safak, E. (1995). Detection and identification of soil-structure interaction in buildings from vibration recordings. *Journal of Structural Engineering*, 121(5), 899-906.

Seo, J., Hu, J. W., & Lee, J. (2016). Summary review of structural health monitoring applications for highway bridges. *Journal of Performance of Constructed Facilities*, *30(4)*.

Sextos, A., Faraonis, P., Zabel, V., Wutke, F., Arndt, T., & Panetsos, P. (2016). Soil-bridge system stiffness identification through field and laboratory measurements. *Journal of Bridge Engineering*, *21(10)*, 1084-0702.

Skarlatoudis, A.A., Papazachos, C.B., Margaris, B.N., Theodoulidis, N., Kalogeras, I, Scordilis, E.M., & Karakostas, V. (2003). Empirical peak ground-motion predictive relations for shallow earthquakes in Greece. *Bulletin of the Seismological Society of America*, *93(6)*, 2591-2603.

Spiridonakos, M., Chatzi, E., & Sudret, B. (2016). Polynomial chaos expansion models for the monitoring of structures under operational variability. *Journal of Risk and Uncertainty in Engineering Systems*, *Part A:Civil Engineering, 2(3)*.

Stewart, J.P., & Fenves, G.L. (1998). System identification for evaluating soil-structure interaction effects in buildings from strong motion recordings. E*arthquake Engineering and Structural Dynamics*, *27(8)*, 869–885.

Stewart, J.P., Conte, J.P., & Aiken, I.D. (1999). Observed behavior of seismically isolated buildings. *Journal of Structural Engineering, 125(9)*, 955–964.

Taskari, O., & Sextos, A. (2015). Effect of the abutment-embankment system stiffness on the seismic response of short bridges. *Journal of Earthquake Engineering*, *19(5)*, 822-846.

Teughels, A., & De Roeck, G. (2004). Structural damage identification of the highway bridge Z24 by FE model updating. *Journal of Sound and Vibration*, *278(3)*, 589-610.

Theodulidis, N., & Papazachos B. (1992). Dependence of strong ground motion on magnitude-distance, site geology and macroseismic intensity for shallow earthquakes in Greece: I, Peak horizontal acceleration, velocity and displacement. *Soil Dynamics and Earthquake Engineering*, *11(7)*, 387-402.

Todorovska, M. (2009). Soil-structure identification of Millikan library north-south response during four earthquakes (1970-2002). What caused the observed wandering of the system frequencies. *Bulletin of the Seismological Society of America*, *99(2A*), 626–636.

Trifunac, M.D., Ivanovic, S.S., & Todorovska, M.I. (2001b). Apparent periods of a building. II: Time-frequency analysis. *Journal of Structural Engineerin*g, *127(5)*, 527-537.

Werner, S.D., Beck, J.L., & Levine, M.B. (1987). Seismic response evaluations of Meloland road overpass using 1979 Imperial Valley earthquake records. E*arthquake Engineering and Structural Dynamics*, *15(2)*, 249-274.

Wu, J.R., & Li, Q.S. (2004). Finite element model updating for a high-rise structure based on ambient vibration measurements. Engineering Structures, *26(7)*, 979-990.

Yuen, K.V., & Kuok, S.C. (2010). Ambient interference in long-term monitoring of buildings. *Engineering Structures*, *32(8)*, 2379-2386.

Yura, J., Kumar, A., Yakut, A., Topkaya, C., Becker, E., & Collingwood, J. (2001) Elastomeric bridge bearings: recommended test methods, National Academy Press, Washigton, DC.

Zhang, J., & Makris, N. (2002). Kinematic response functions and dynamic stiffnesses of bridge embankments. E*arthquake Engineering and Structural Dynamics*, *31(11)*, 1933–1966.

Zivanovic, S., Pavic, A., & Reynolds, P. (2006). Finite element modelling and updating of a lively footbridge: The complete process. *Journal of Sound and Vibration*, *301(1-2)*, 126-145.

Table 1. Identified versus finite element model (FEM) predicted natural frequencies f and mode shape deviations (MAC) of Kavala bridge (w stands for the contribution level of the mode shapes in the objective function $J(\theta)$).

		Numerically predicted							
				Updated					
				Case A		Case B		Case C	
	Identified	Nominal		w=1		w=0.5		w=0	
	Ambient Vibrations	FEM		FEM A		FEM B		FEM C	
Mode no[a]	f(Hz)	f(Hz)	MAC	f(Hz)	MAC	f(Hz)	MAC	f(Hz)	MAC
1 (T1)	0.81	0.54	0.94	0.80	0.99	0.81	0.99	0.82	0.99
2 (L1)	1.29	0.57	0.97	1.23	0.97	1.23	0.97	1.24	0.97
3 (T2	1.61	0.67	0.94	1.66	0.97	1.66	0.97	1.65	0.97
4 (T3)	2.36	1.23	0.89	2.44	0.97	2.43	0.97	2.41	0.97
5 (B1)	3.41	3.03	0.99	3.39	0.99	3.38	0.99	3.37	0.99
6 (B2)	3.46	3.09	0.76	3.45	0.99	3.44	0.99	3.43	0.99
7(B3)	3.51	3.19	0.79	3.51	1.00	3.50	1.00	3.50	1.00
Average error[b]		32.34%		1.89%		1.78%		1.72%	

[a] T, L and B are the transverse, longitudinal and bending modes of the deck, respectively.

[b] $\left(\sum_{i=1}^{n} \left| \frac{f_{Identified,i} - f_{Numerical,i}}{f_{Identified,i}} \right| \Big/ n \right) \times 100$, where $i^{th} = \{1,\ldots,n\}$ the number of mode .

Table 2. Nominal material mechanical properties[a] of the developed numerical model.

Elements	Material	E (kN/m^2)	v	ρ (t/m^3)
Superstructure				
Deck	Concrete	$34 \cdot 10^6$	0.20	4.58
I-beams	Concrete	$34 \cdot 10^6$	0.15	2.5
Bearings				
Elastomeric part	Elastomeric	3600 (G=1200kN/m^2)	0.50	1.3
Steel plates	Steel	$200 \cdot 10^6$	0.30	7.85
Substructure				
Piers	Concrete	$30 \cdot 10^6$	0.20	2.5
Caissons	Concrete	$30 \cdot 10^6$	0.20	2.5
Abutments	Concrete	$30 \cdot 10^6$	0.20	2.5
Soil				
Abutment subsoil	Rock	$3.5 \cdot 10^6$	0.30	2
Pier subsoil	Rock	$3.5 \cdot 10^6$	0.30	2
Embankments	Rock	$3.5 \cdot 10^6$	0.30	2
Abutment backfill	Artificial soil (compacted)	$60 \cdot 10^3$	0.30	2

[a] Young's modulus of elasticity E, Poisson ratio ν, mass density ρ and shear modulus G.

Table 3. Selected model updated parameters and model updating results for the three studied Cases (E stands for Young's modulus of elasticity and w stands for the contribution level of the mode shapes in the objective function $J(\theta)$).

Parameters	Location	Symbols[a]	Constraints	Case A w=1	Case B w=0.5	Case C w=0
E	Deck[b]	θ_{deck}	0.70-1.30	1.21	1.20	1.19
E	Piers[c]	θ_{piers}	0.70-1.30	1.12	1.18	1.25
E	Bearings[d]	θ_{bear}	1-15	11.99	11.83	11.63

[a] $\theta = \dfrac{\text{updated value}}{\text{nomnal value}}$.

[b] Including the deck and the I-beams.

[c] Including the piers M_1, M_2 and M_3.

[d] Including the bearings of the piers and the abutments (only the elastomeric part).

Table 4. Optimal solutions obtained from alternative optimization algorithms.

Optimal solution		CMA-ES	fminsearch	fmincon	fminunc
θ_{deck}		1.197	1.197	1.214	1.206
θ_{piers}		1.180	1.183	1.133	1.144
θ_{bear}		11.83	11.84	11.94	11.89
f(value)		0.0652974	0.0652969	0.0655806	0.0653774
stopping criteria	f tolerance	10^{-6}	10^{-6}	10^{-6}	10^{-6}
	max $No._{eval}$	500	300	300	300
total $No._{evaluations}$		300	184	187	184

Table 5. Response spectrum analysis results at the base of pier M_1 founded on soil type B.

Combinations		N(kN)	Qy(kN)	Mz(kNm)	Qz(kN)	My(kNm)
1.35G+1.5Q		-22760	-51	-1151	0	0
G+0.2Q±0.3Ex±Ey±0.3Ez	max	-14910	+231	+6594	+724	+22199
	min	-15910	-300	-6181	-724	-22199

Table 6. Response spectrum analysis results at the base of pier M_1 founded on soil type C.

Combinations		N(kN)	Qy(kN)	Mz(kNm)	Qz(kN)	My(kNm)
1.35G+1.5Q		-22759	-48	-1133	0	0
G+0.2Q±0.3Ex±Ey±0.3Ez	max	-14121	+232	+6273	+704	+21500
	min	-15882	-297	-5965	-704	-21500

List of Figures

Figure 13. Influence of alternative soil foundation stiffness on the first seven mode shapes of the Kavala bridge (T: transverse mode, L: longitudinal mode, B: bending mode).

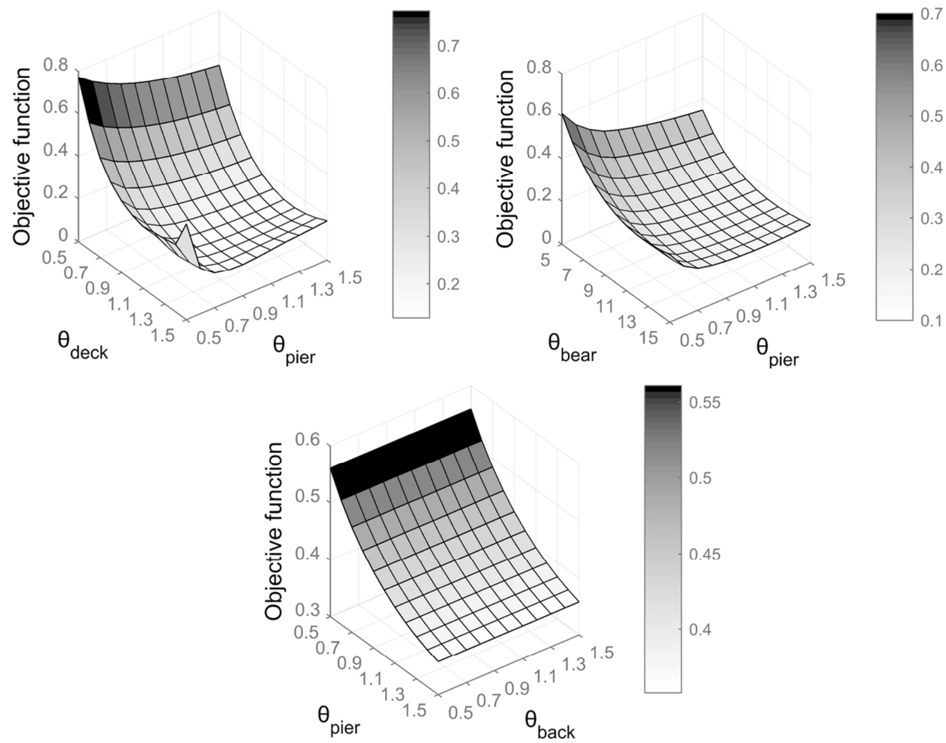

Figure 1. Objective function plot.

119x92mm (300 x 300 DPI)

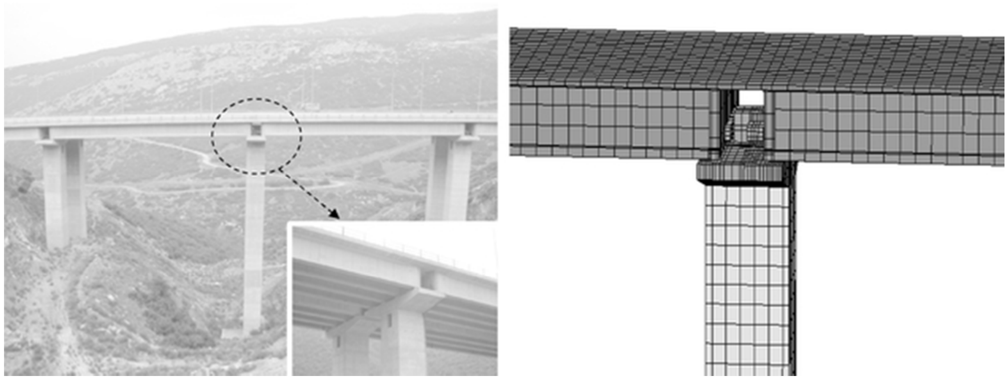

Figure 2. General overview of the 2nd Kavala Ravine bridge, detail of the pier-deck connection (left) and FE representation of the continuity slab (right).

53x21mm (300 x 300 DPI)

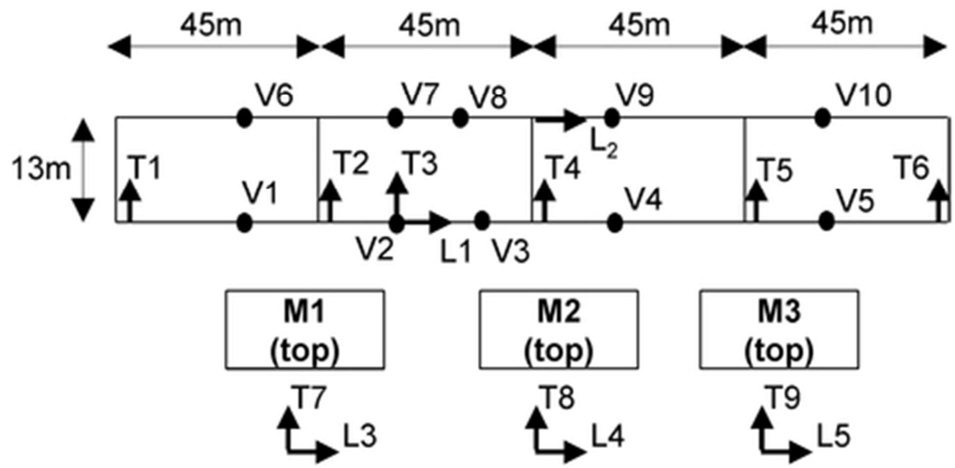

Figure 3. Instrumentation of the Kavala bridge according to Ntotsios et al., 2008.

41x19mm (300 x 300 DPI)

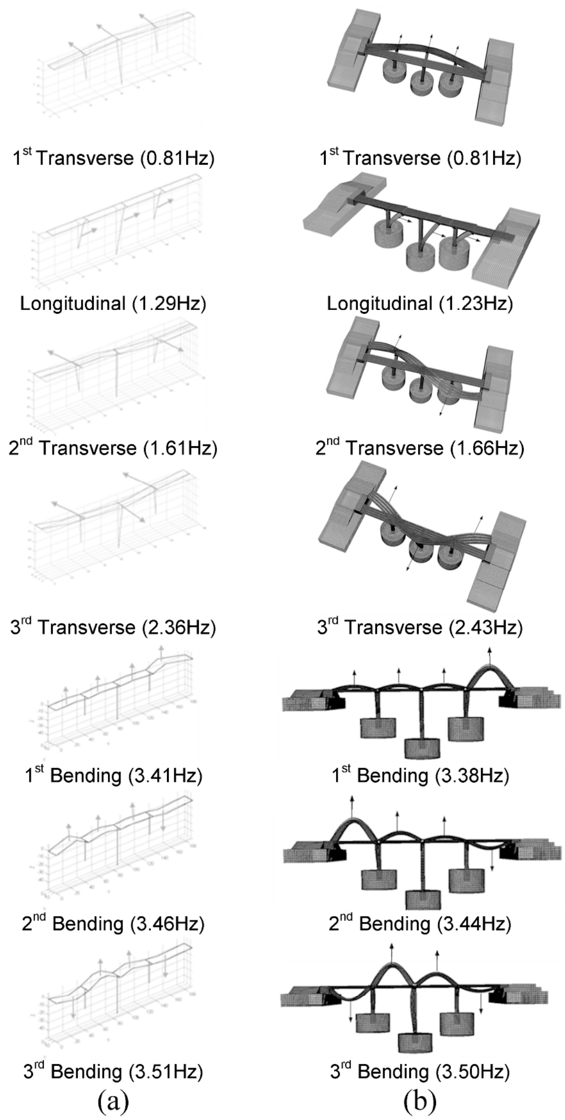

Figure 4. (a) Identified mode shapes of Kavala bridge (Ntotsios et al., 2008) and (b) numerically predicted mode shapes of its updated 3D numerical model (FEM B).

171x334mm (300 x 300 DPI)

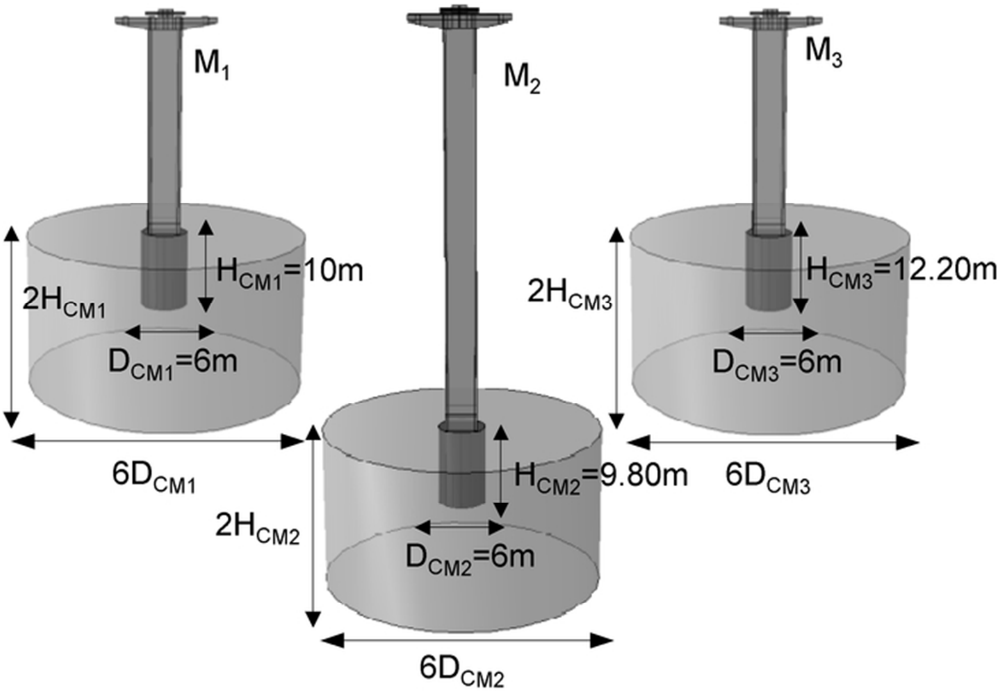

Figure 5. Modelling details of the embedded caisson foundations of piers M1, M2 and M3.

61x43mm (300 x 300 DPI)

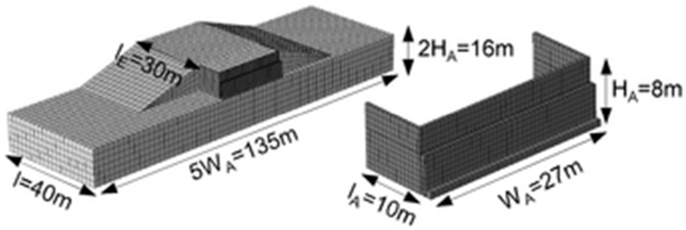

Figure 6. Modelling details of the abutment-backfill-embankment system.

29x10mm (300 x 300 DPI)

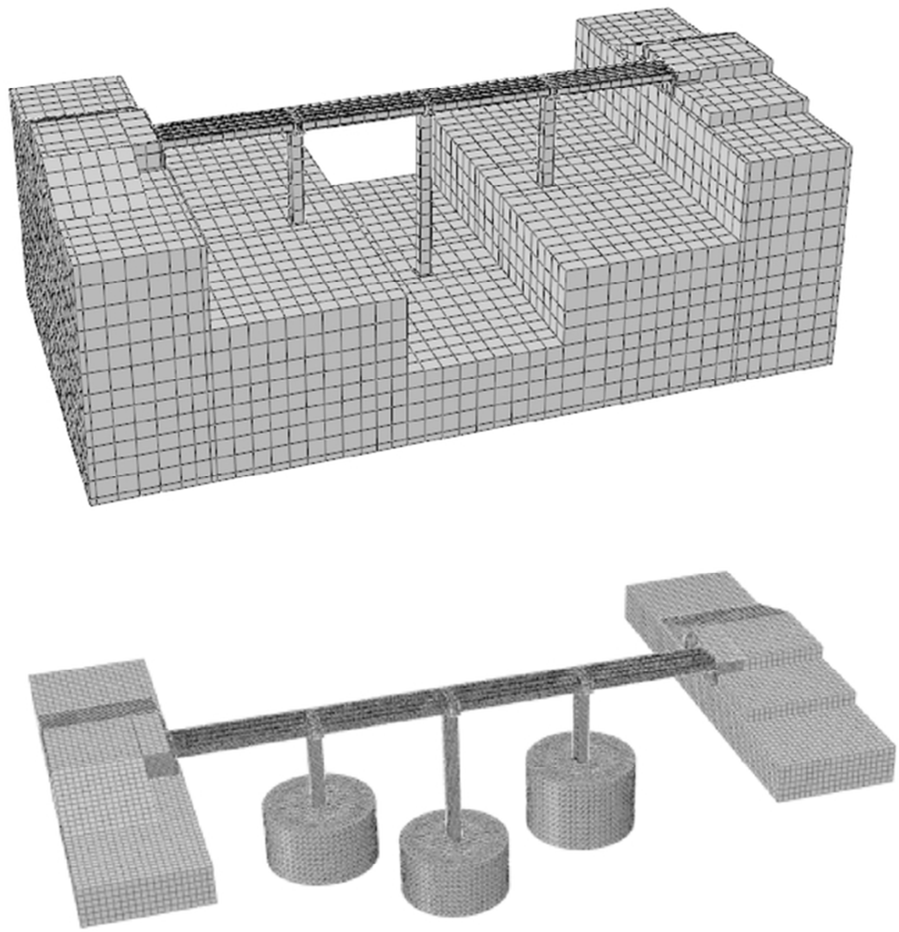

Figure 7. Refined bridge-soil FE model (top) compared to FE model used in the analysis (bottom).

60x59mm (300 x 300 DPI)

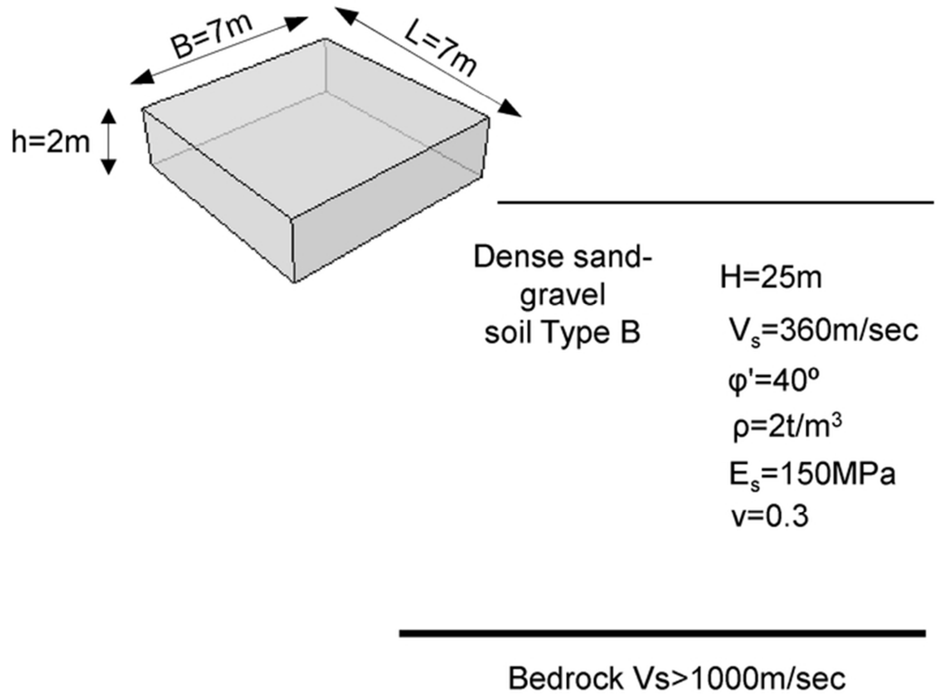

Figure 8. Shallow foundation geometry details founded on examined soil profile type B (H=height, Vs=shear wave velocity, φ'=effective friction angle, ρ=density, Es=unconfined compression modulus, v=Poisson's ratio)

64x47mm (300 x 300 DPI)

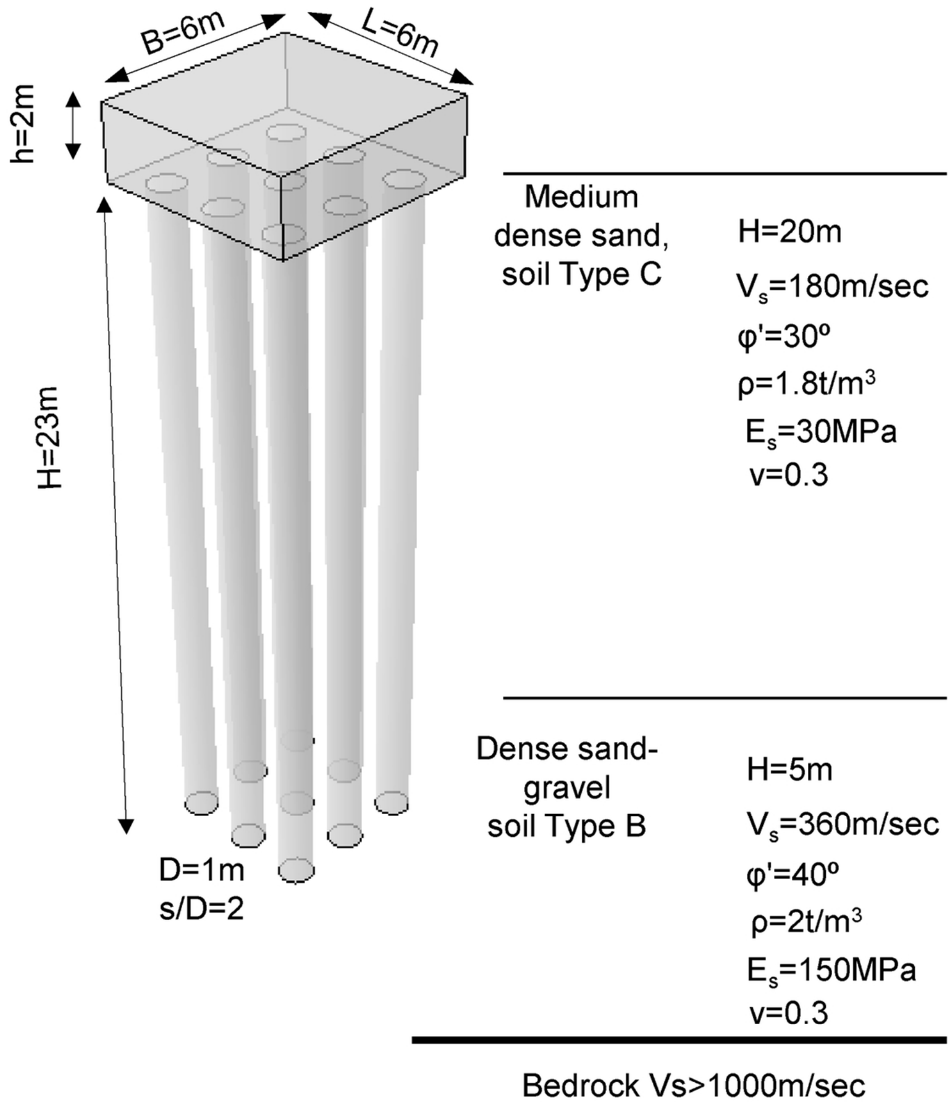

Figure 9. Pile group-pile cap geometry details founded on examined soil profile type C (H=height, Vs=shear wave velocity, φ'=effective friction angle, ρ=density, Es=unconfined compression modulus, v=Poisson's ratio).

99x114mm (300 x 300 DPI)

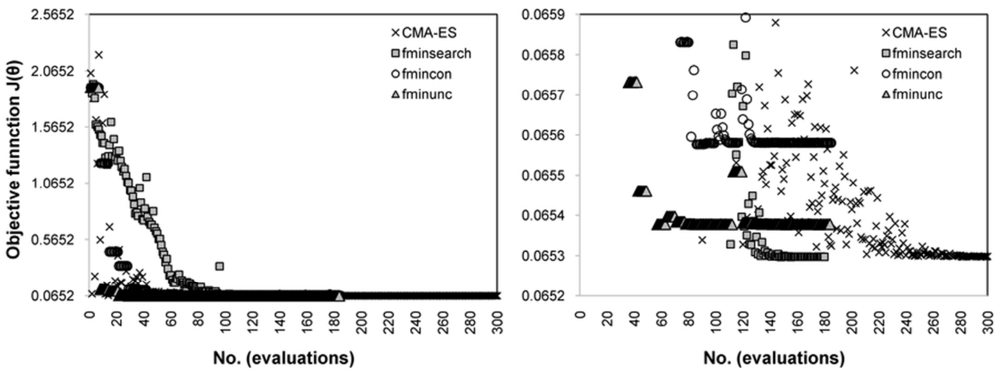

Figure 10. Minimization of objective function J(θ) with alternative algorithms.

76x29mm (300 x 300 DPI)

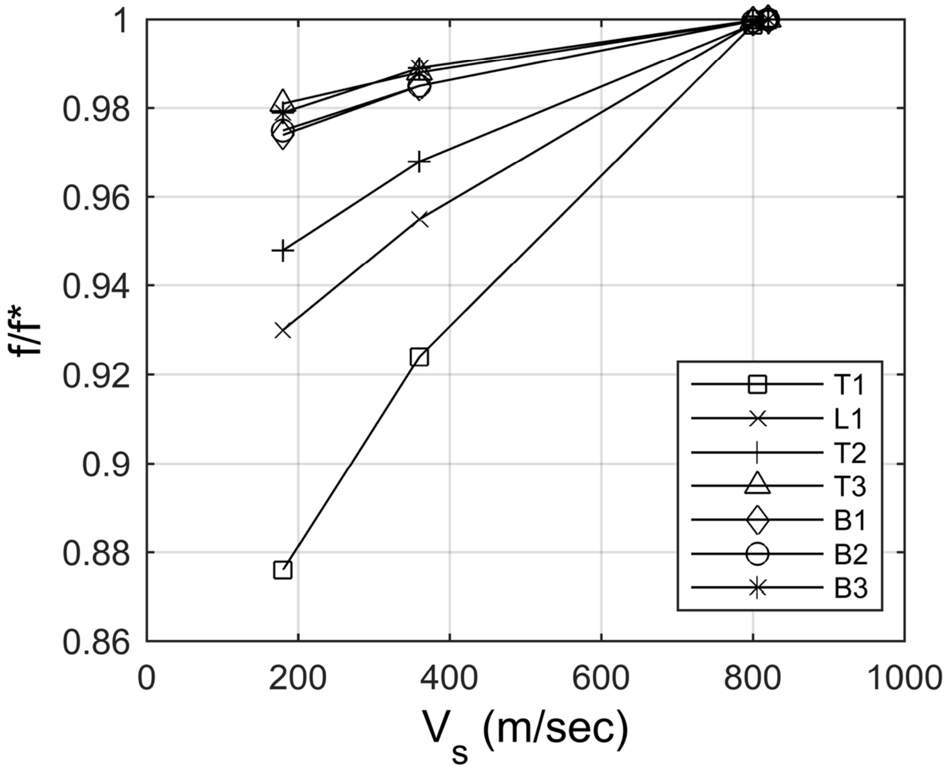

Figure 11. Influence of alternative soil-foundation stiffness on the first seven natural frequencies of the Kavala bridge (T: transverse mode, L: longitudinal mode, B: bending mode).

64x52mm (600 x 600 DPI)

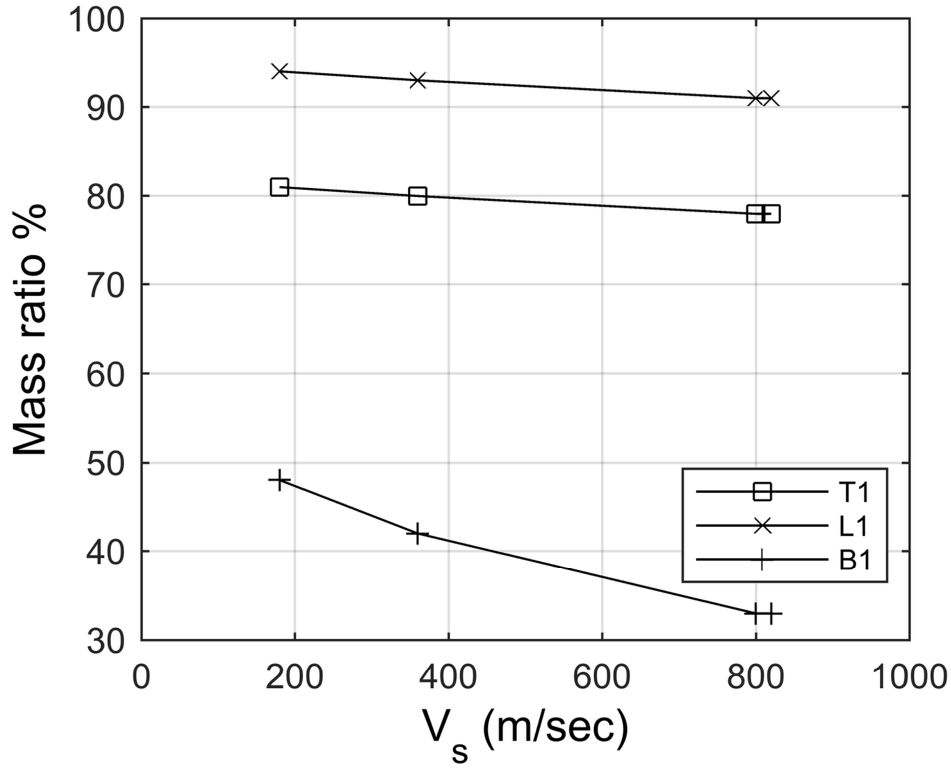

Figure 12. Influence of alternative soil-foundation stiffness on the modal participating mass ratios of Kavala bridge first longitudinal (L1), transverse (T1) and bending (B1) modes.

64x52mm (600 x 600 DPI)

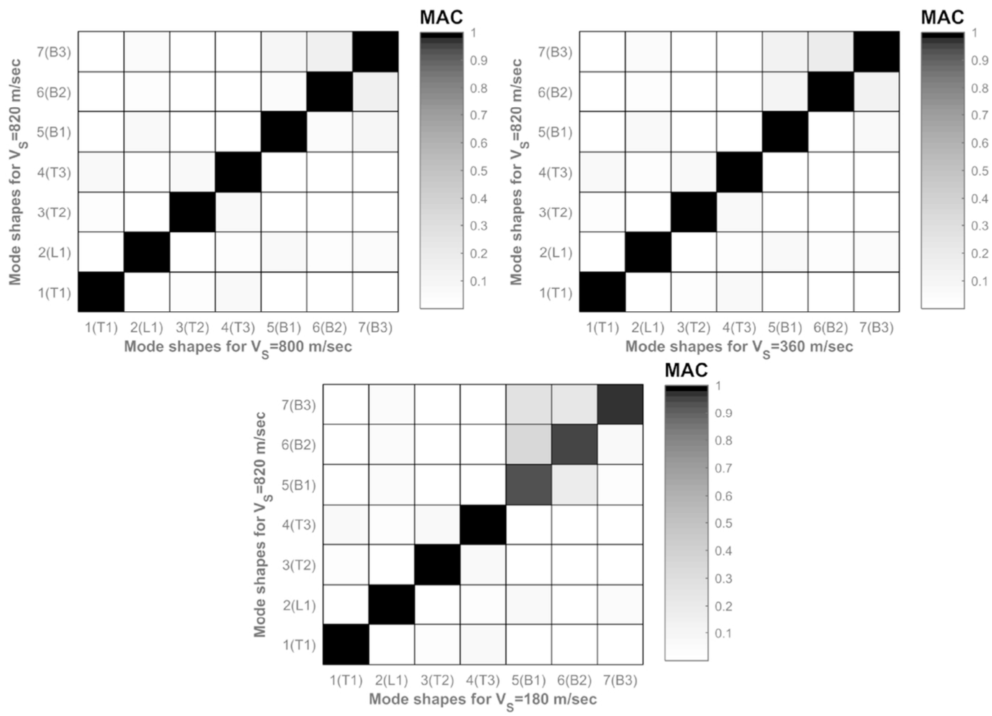

Figure 13. Influence of alternative soil foundation stiffness on the first seven mode shapes of the Kavala bridge (T: transverse mode, L: longitudinal mode, B: bending mode).

116x83mm (300 x 300 DPI)